An Observational Study of the Coastal Barrier Jet Induced by a Landfalling Typhoon and its Influence on Precipitation and Intensity Changes

Yu-Cheng Kao and Ben Jong-Dao Jou

Department of Atmospheric Sciences, National Taiwan University, Taipei, Taiwan

ynow37@gmail.com

Abstract

The coastal barrier jet (CBJ) induced in typhoon environment is a critical mesoscale phenomenon that causes significant precipitation structure and intensity change of typhoon prior to its landfall in Taiwan area. By using coastal Doppler radar and surface observations in Taiwan, CBJ and precipitation structure and intensity changes of typhoon Haitang (0505) before landfall are studied.

It is found that the formation and evolution of CBJ was controlled by different flow regimes associated with Haitang. When outer circulation touched the coastal terrain, CBJ formed. A persistent prevailing strong northeasterly wind impinging the mountain led to the formation of CBJ parallel to the shore. The CBJ persisted for almost 6 h and was approximately 140 km long and 25 km wide. The northern branch of the CBJ had a stronger wind (maximum wind speed > 50 m s^{-1}), a greater vertical extent (the core of the CBJ was between 1.0 and 2.5 km in height), and a more persistent jet signal than the southern branch (maximum wind speed ~ 45 m s^{-1} and the core was between 1.0 and 2.0 km). After the core region reached the coastal terrain, considerable curvature of the core region circulation caused the southern branch of CBJ shifted offshore.

The northerly CBJ and the southerly of the terrain-induced leeside mesolow (located to the southeast of topography) converged at southwest portion of the storm center resulting an east-west line convection, approximately 160 km in length and 20 km in width, formation. The line convection moved cyclonically and merged into inner eyewall lead to the concentric eyewall breakdown and temporal weakening of the storm. When Haitang moved to approximately 60 km off the coast, the western-side eyewall recovered by nearshore convection, and followed eyewall contraction and re-intensification.

Key word: landfalling typhoon, coastal barrier jet, leeside mesolow, eyewall breakdown

1. Introduction

Typhoons are the most threatening weather system in the area around Taiwan. Because of the complex interaction between typhoon circulation and terrain, dramatic changes in trajectory, intensity, circulation, and precipitation are expected when typhoon approaching the island and render precise forecasting of typhoons highly challenging (Wu and Kuo 1999). The numerous numerical simulation studies shows that the coastal barrier jet (CBJ) is one of the prominent terrain-induced mesoscale phenomena that can significant affect the track and inner-core structure of westbound landfalling typhoon (Jian and Wu 2008; Huang et al. 2011; Lin et al. 1999). However, the detailed documentation of CBJ and precipitation and intensity changes associated with landfalling typhoon from an observational perspective is still lacking.

Typhoon Haitang is the fifth typhoon of the 2005 Northwest Pacific typhoon season (0505) and a super typhoon with a looping track before its made landfall. When Haitang was approaching Taiwan Island, a coastal barrier jet (CBJ) and dramatic precipitation structure change including line convection formation, concentric eyewall breakdown, eyewall reorganization, and contraction were observed. This study aims to document the structure evolution and identify the physical processes of the formation mechanism of CBJ, examine the precipitation structure and intensity change of Haitang, and clarify the role of CBJ on Haitang precipitation and intensity changes.

2. Data and Methodology

The data sets used in this study including land-based Doppler Radar data, surface stations data and sounding station data are summarized in Fig. 1. The observations from the radar network of Central Weather Bureau (CWB) operational S-band Doppler radar are used to document the CBJ and the precipitation structure evolution of Haitang. The hourly wind, temperature, and pressure observations of 120 surface stations around the Taiwan Island are used to analyze the mesoscale airflow and pressure field during Haitang landfall period. Sounding data from Hua-lien (466990) is used to estimate the Brunt–Väisälä frequency for Froude number calculation.

The extended VAD technique (Srivastava et al 1986) that can retrieve the vertical profile of the horizontal wind is applied in Hua-lien radar (RCHL) data to identify the CBJ. The generalized velocity track display (GVTD) technique (Jou et al. 2008) is performed to retrieve TC circulation including axisymmetric tangential and radial winds and high wavenumber tangential winds to estimate the storm intensity evolution.

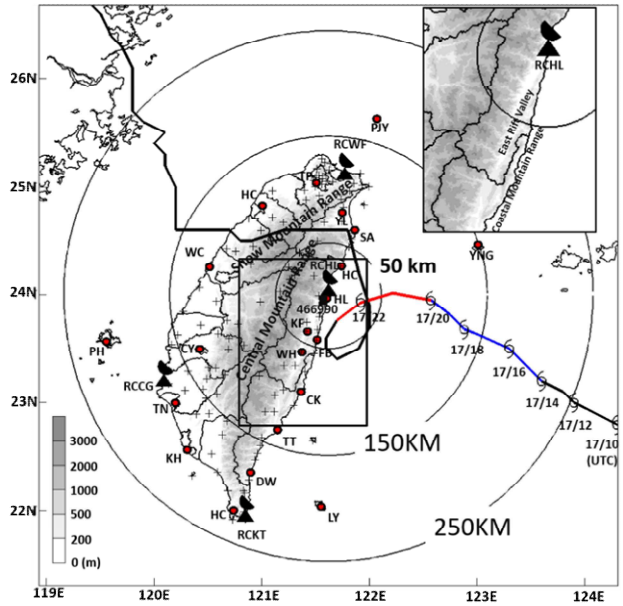

Fig. 1. Best track of Typhoon Haitang (0505) and various observations used in this study. Blue + red segment represents defining CBJ period, and red segment represents the significant structure change period of Haitang.

3. Results and Discussions

a. CBJ characteristics

Fig. 2a is the average horizontal wind vertical profile during the CBJ period (31 data points matched wind speed and vertical wind shear criteria). The average maximum wind speed indicates the height of the maximum wind is at 2.5 km and with a magnitude of 41.9 m s^{-1} a standard deviation 1.9 m s^{-1}, therefore the wind speed threshold of the CBJ at 2.5-km height is defined as 40 m s^{-1} (average maximum wind speed minus one standard deviation). Fig. 2b displays the occurrence frequency of Vr over 40 m s^{-1} at 2.5-km height during the CBJ period, i.e., the number of pixels with Vr > 40 m s^{-1} and the maximum number is 31. The generally feature of the CBJ is clearly depicted. The CBJ is located along the east coast in a terrain-parallel direction and is approximately 140 km long and 25 km wide. The CBJ occurrence frequency is higher in the northern branch implying greater persistence over time. The composite vertical cross-section of the maximum Vr along the axis of the CBJ (Fig. 2c) shows stronger wind

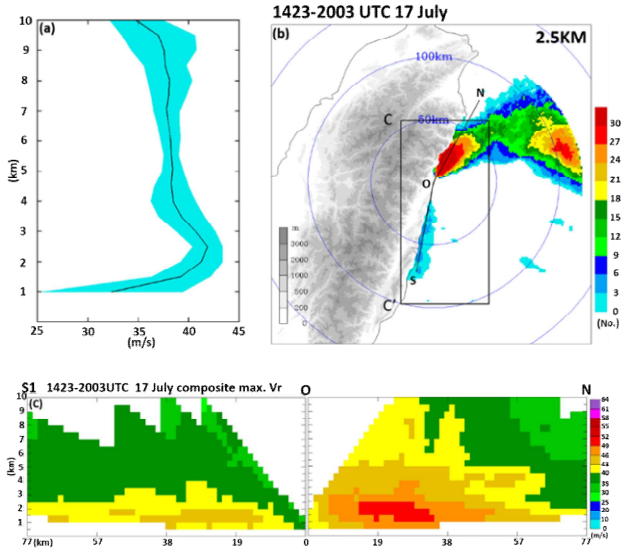

Fig. 2. (a) Vertical wind profile during the CBJ period (black line is average, light blue shading shows the standard deviation). (b) Frequency of horizontal distribution of Doppler radial velocity (V_r) over 40 m s^{-1} at 2.5-km altitude. The rectangular box indicates the analysis domain of the temporal evolution of the CBJ. Black lines $\overline{ON}$ and $\overline{OS}$ indicate the direction of the cross sections in (c). (c) Composite maximum V_r along the line $\overline{ON}$ and $\overline{OS}$ in (b) during the CBJ period.

The composite vertical cross-section of the maximum Vr along the axis of the CBJ (Fig. 2c) shows stronger wind speeds (maximum wind speed 49–52 m s^{-1}) and a greater

vertical extent (core of the jet is located at 1.0–2.5 km in height) along the northern branch. By contrast, weaker wind speeds (maximum wind speed 43–46 m s^{-1}) and a smaller vertical extent (core of the jet is located at 1.0–2.0 km in height) are noted along the southern branch.

The result of Froude number (F_r = U/NH, where U is the upstream wind speed normal to the mountain, N is the Brunt–Väisälä frequency, and H is the terrain height) estimation during CBJ period is between 0 and 0.75 further supporting the terrain blocking effect is the formation mechanism of CBJ (Kao et al. 2019).

b. CBJ evolution

The evolution of the CBJ is investigated by examining the temporal variation in the maximum Vr at 2.5-km altitude along the long axis of the selected domain (black rectangular box in Fig. 2b) covering the CBJ horizontal extent between almost 26 hours prior to Haitang landfall (Fig. 3). Period I was the formation stage, intermittent strong wind speed (>20 m s^{-1}) associated with passing rainbands was the main feature. Period II, the intensifying stage, the considerable increase of Vr over time was the major feature. Period III was the mature stage, the analysis domain was covered by core region of Haitang and the CBJ signal with Vr > 40 m s^{-1} began to dominate. Two distinct features can be identified in this period. Before 1613 UTC, the CBJ extended in the meridional direction both north and south and with much stronger Vr in the northern branch than the southern branch. After 1613 UTC, the area with Vr > 45 m s^{-1} became persistent in the northern branch. However, the CBJ signal south of HL disappeared. Once the core region of Haitang had reached the coast (1803 UTC), the meridional extent of the CBJ began to decrease, that is the Vr > 30 m s^{-1} area shrank. The shrinkage was associated with formation of intense convection south of Haitang's center. Period IV was the final stage, the analysis domain was influenced by the eyewall, and the CBJ signal decayed significantly.

The analysis result shows that the formation and evolution of CBJ was controlled by different flow regimes associated with Haitang. When outer circulation (with a small curvature and quasi-steady state, i.e., relative weaker vorticity) of Haitang touched the coastal terrain, the persistent strong northeasterly wind impinged the coast and a terrain-parallel orientation of the CBJ was generated. When the core region approached the coastal terrain, the considerable curvature of core-region circulation started to affect the coast, and stronger vorticity changed the CBJ structure, with the southern branch of the CBJ shifting offshore. This shift resulted in disappearance of strong wind on the south side of the radar after 1803 UTC 17 July.

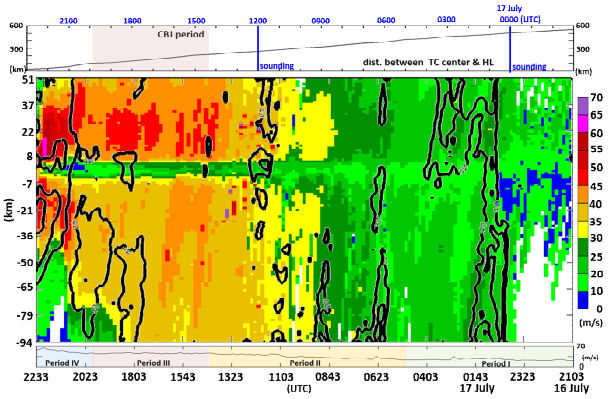

Fig. 3. Temporal variation of maximum V_r (shading) in direction normal to the long axis of the rectangular box marked in Fig. 2b at 2.5-km altitude between 2103 UTC 16 July and 2233 UTC 17 July. Abscissa is time, and ordinate is distance to RCHL, positive (negative) indicating to the north (south) of RCHL. Black contour is maximum reflectivity in direction normal to the long axis over a 40-dBZ area. Maximum wind speed over the four periods (Period I-IV) is depicted in the lower panel. Distance between the typhoon center and HL is depicted in the upper panel.

c. The precipitation changes of Haitang

The precipitation structure of Haitang underwent a dramatic change while the storm center was within 120 km to the coast. Starting from a symmetric pattern, subsequently, merged with line convection, breakdown of concentric eyewall, and finally, eyewall axisymmetrization and contraction. Fig. 4 is a series of composite reflectivity images during 3 hours period after the formation of line convection (correspond to the red segment depicted in Fig. 1). At 1930 UTC, the concentric

eyewall feature was still recognizable. Moreover, an east-west orientation line convection, which is approximately 160 km in length and 20 km in width, formed south to the storm center and connected to the outer eyewall. At 2000 UTC, the line convection separated from the outer eyewall and moved radial inward to connect with inner eyewall. At 2030 UTC, the eastern semicircle of inner eyewall convection was enhanced significantly, and the western portion of eyewall vanished, i.e., the concentric eyewall broke down. At 2100 UTC, line convection kept its cyclonic motion and shifted gradually to the east. On the other hand, the reflectivity between 30-60 km radii to the northwest portion of the storm center was enhanced. At 2130 UTC, a significant wave number two inner-core reflectivity structure formed, with peak reflectivity located at the west and east side. At 2230 UTC, the eyewall contracted radial inward significantly (from 45 to 20 km radius) and posed an annular shape (become axisymmetric) with more intense convection.

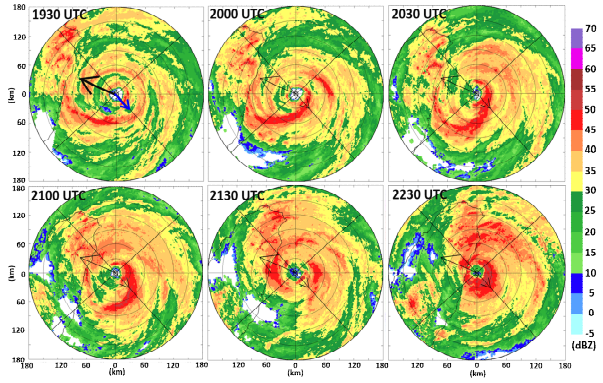

Fig. 4. Composite reflectivity images within 180 km radius from storm center at 1930, 2000, 2030, 2100, 2130, and 2230 UTC. Black (blue) arrow indicates motion (shear) vector.

d. The intensity changes of Haitang

Accompanying with the significant precipitation structure evolution, the dramatic intensity change of the storm was expected. When the inner-core region of Haitang was within 110 km distance to the coast, the GVTD technique was suitable to retrieve primary circulation and estimate the intensity evolution. Fig. 5 is the radius profiles of mean reflectivity, mean tangential wind and its derived quantities relative vertical vorticity ($\bar{\eta} = \bar{V}_t/r + \partial\bar{V}_t/\partial r$) and pressure perturbation ($\bar{V}_t^{\,2}/r + f\bar{V}_t = (1/\overline{\rho})\,(\partial\bar{p}'/\partial r$), the gradient wind balance assumption) field at 2 km altitude in five specific analysis times. Between 1933 and 2033 UTC (the concentric eyewall breakdown period), the reflectivity profiles reveal a double peak feature (concentric eyewall feature) and inner peak increase with time (reflect the line convection merged into inner eyewall). In contrast, the corresponding mean tangential wind decrease, this feature indicates the weakening of storm. Between 2033 and 2103 UTC, the mean tangential wind began to intensify (maximum wind speed at RMW, increased from 35.3 to 47.7 m s^{-1}) and the maximum mean reflectivity shifted radial outward from 22 to 55 km radius from the storm center (corresponding to the intense reflectivity recovering in the north-western periphery to the storm center). By 2123 UTC, the west periphery eyewall redeveloped, and the reflectivity image revealed striking asymmetric wave number two structure. At this moment, the mean tangential wind further increased from 47.7 to 59.8 m s^{-1}. After 2123 UTC, the asymmetric wave number two structure transformed into an axisymmetric one i.e. underwent an axisymmetrization

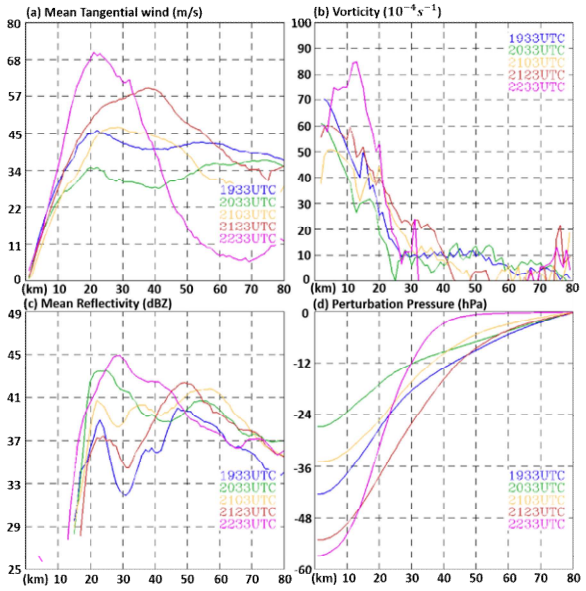

Fig. 5. The radial profiles of mean tangential wind (a), vertical vorticity (b), mean reflectivity (c), and perturbation pressure (d) within 80 km radius from the storm center at 1933, 2033, 2103, 2123, and 2233 UTC.

process and associated with significant eyewall

contraction and intensification. The maximum mean tangential wind speed reached 70.8 m s^{-1} and the RMW shrunk from 38 to 21 km radius from the storm center. Rodgers et al. (2016) suggested that the increased azimuthal coverage of intense convection leads to a greater symmetry of diabatic heating and is a favorable configuration for vortex spin-up. The re-developed western periphery deep convection and re-intensification process of Haitang resemble to the concept proposed by Rodgers et al. (2016). Moreover, the radial profile of vertical vorticity evolved from a monotonic one to an annular one. The annular vertical vorticity ring is typically indicative of intensifying tropical cyclone (Kossin and Eastin 2001).

e. The role of CBJ

The analysis results mentioned above reveal that the formation of an east-west orientation line convection south to the storm center played a crucial role in precipitation structure modification and accompanied intensity variation of Haitang. The line convection formed while the southern brand of CBJ was shifting offshore, therefore, it is reasonable to speculate that the CBJ has a role in the formation of line convection.

Fig. 6 is the surface pressure anomaly and wind field around the island overlaid with composited reflectivity from the CWB radar network at 2000 UTC 17 July. The storm center located approximately 100 km from the east coast and intense line convection appeared in the southwest to south quadrant. In the east of the island, strong northerly flow (i.e. the CBJ) along the coast to the north of HL, a mesolow (pressure anomaly reaches -33 hPa) formed near TT and CK due to subsidence of downslope northwesterly flow. A significant weak reflectivity area, resulting from convection suppression, collocated with mesolow is the evidence of subsidence. The southerly flow at TT and DW (associated with mesolow) contradicting to the northerly flow at HL, that is, the airflow converged between HL and CK providing a favor environment for line convection initiation.

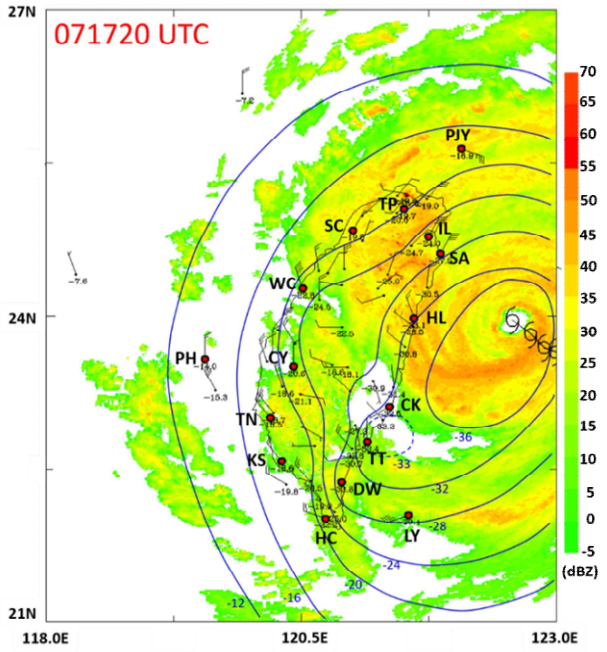

Fig. 6. The mesoscale surface pressure and circulation field at 2000 UTC 17 July. The contour line is pressure anomaly field (difference from hourly average station pressure during 2001-2010, the interval is 4 mb), shading area is composite reflectivity from CWB radar network.

Fig. 7 is temporal variation of positive and negative V_r overlaid with derived divergence at 1.5 km altitude, the analysis domain focus on the south of RCHL (between O and C' of rectangular box in Fig. 2b). The convergent zone

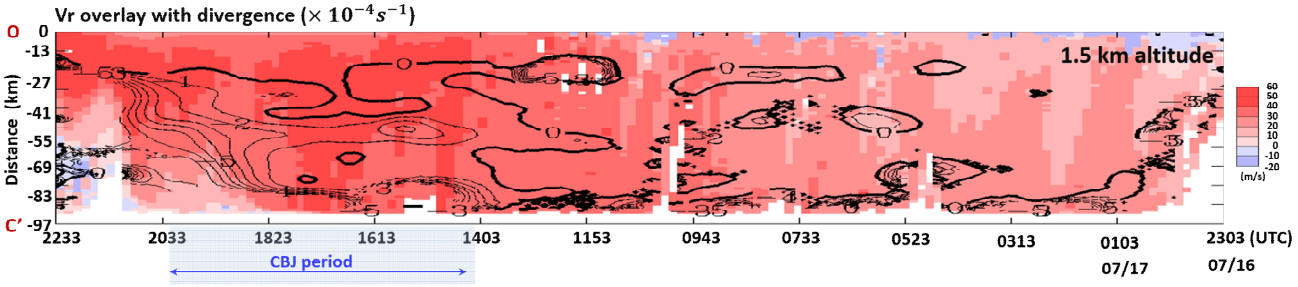

Fig. 7. Temporal variation of maximum V_r (shading, positive and negative indicating northerly and southerly flow respectively) overlaid with the divergence (contour, unit is 10^{-4} s^{-1}) at 1.5 km altitude south to the RCHL.

located between 27 and 97 km south to the RCHL during the CBJ period. The magnitude of convergence increased significantly when the southern branch of CBJ began to shrink northward and associated with the appearance of southerly flow. This result provides direct proof that the line convection is induced in a convergent zone consistsof CBJ northerly flow and mesolow southerly flow.

4. Conclusions

The coastal barrier jet (CBJ) induced in the typhoon environment, a unique mesoscale phenomenon in the Taiwan area is studied from the observational perspective for the first time. The role of CBJ on the precipitation structure and intensity changes of typhoon Haitang is also explored.

It is found that the formation and evolution of CBJ was controlled by different flow regimes associated with Haitang. When outer circulation touched the coastal terrain, CBJ formed. A persistent prevailing strong northeasterly wind impinging the mountain led to the formation of CBJ parallel to the shore. The CBJ persisted for almost 6 h and was approximately 140 km long and 25 km wide. The northern branch of the CBJ had a stronger wind (maximum wind speed > 50 m s^{-1}), a greater vertical extent (the core of the CBJ was between 1.0 and 2.5 km in height), and a more persistent jet signal than the southern branch (maximum wind speed ~ 45 m s^{-1} and the core was between 1.0 and 2.0 km). After the core region reached the coastal terrain, considerable curvature of the core region circulation caused the southern branch of CBJ to shift offshore.

The precipitation modification and intensity fluctuation of Haitang are closely related to the terrain-induced CBJ and leeside mesolow. The northerly CBJ and the southerly of mesolow converged at the southwest portion of the storm while Haitang was approximately 100 km off the east coast. East-west line convection, approximately 160 km in length and 20 km in width, formed in convergent zone. Then, the line convection moved cyclonically and merged with the inner eyewall, caused the breakdown of concentric eyewall and temporal weakening of the storm. Following the concentric eyewall breakdown, the storm underwent an axisymmetrization process with significant eyewall contraction and intensification. The maximum mean tangential wind speed reached ~70 m s^{-1} and the radius of maximum wind shrunk from 38 to 21 km.

Acknowledgement

The authors would like to thank the Ministry of Science and Technology for their funding support (MOST-109-2119-M-002-016), and appreciate Central Weather Bureau to provide the radar data.

Reference

Huang, Y.-H., C.-C. Wu, and Y. Wang, 2011: The influence of island topography on typhoon track deflection. *Mon. Wea. Rev.*, **139,** 1708-1727.

Jian, G.-J., and C.-C. Wu, 2008: A numerical study of the track deflection of Super-Typhoon Haitang (2005) prior to its landfall in Taiwan. *Mon. Wea. Rev.*, **136,** 598-615.

Jou, B. J.-D., W.-C. Lee, S.-P. Liu, and Y.-C. Kao, 2008a: Generalized VTD retrieved of atmospheric vortex kinematic structure. Part I: Formulation and error analysis. *Mon. Wea. Rev.*, **128,** 1925-1936.

Kao, Y.-C., B. J.-D. Jou, J. C.-L. Chan and W.-C. Lee, 2019: An observational study of a coastal barrier jet induced by a landfalling typhoon. *Mon. Wea. Rev.*, **147**, 4589-4609.

Kossin, J. P., and M. D. Eastin, 2001: Two distinct regimes in the kinematic and thermodynamic structure of the hurricane eye and eyewall. *J. Atmos. Sci.*, **58,** 1079-1090.

Lin, Y.-L., J. Han, D. W. Hamilton, and C.-Y. Huang, 1999: Orographic influence on a drifting cyclone. *J. Atmos. Sci.*, **56**, 534-562.

Rogers, R., J. A. Zhang, J. Zawislak, H. Jiang, G. R. Alvey and E. J. Zipser, 2016: Observations of the Structure and Evolution of Hurricane Edouard (2014) during Intensity Change. Part II: Kinematic Structure and the Distribution of Deep Convection. *Mon. Wea. Rev.*, **144**, 3355–3376.

Srivastava, R. C., T. J. Matejka, and T. J. Lorello, 1986: Doppler radar study of the trailing anvil region associated with a squall line. *J. Atmos. Sci.*, **43**., 356-377.

Wu, C.-C. and Y.-H. Kuo, 1999: Typhoons affecting Taiwan: current understanding and future challenges. *Bull. Amer. Meteor. Soc.*, **80**, 67-80.